

Article

Improvement of Lithium Storage Performance of Silica Anode by Using Ketjen Black as Functional Conductive Agent

Guobin Hu ^{1,†}, Xiaohui Sun ^{1,†}, Huigen Liu ¹, Yaya Xu ¹, Lei Liao ^{2,*}, Donglei Guo ², Xianming Liu ³ and Aimiao Qin ^{1,*}

¹ Key Lab New Processing Technology for Nonferrous Metal and Materials Ministry of Education, College of Material Science and Engineering, Guilin University of Technology, Guilin 541004, China; kokpinhu@hotmail.com (G.H.); 15564222794@139.com (X.S.); huigenliugz@163.com (H.L.); xuyayachonga@163.com (Y.X.)

² Guangxi Key Laboratory of Environment Pollution Control Theory and Technology, College of Environmental Science and Engineering, Guilin University of Technology, Guilin 541004, China; gdl0594@163.com

³ Key Laboratory of Function-Oriented Porous Materials, College of Chemistry and Chemical Engineering, Luoyang Normal University, Luoyang 471934, China; myclxm@163.com

* Correspondence: fangqiu2001@163.com (L.L.); qam2005032@glut.edu.cn (A.Q.)

† These authors contributed equally to this work.

Abstract: In this paper, SiO₂ aerogels were prepared by a sol–gel method. Using Ketjen Black (KB), Super P (SP) and Acetylene Black (AB) as a conductive agent, respectively, the effects of the structure and morphology of the three conductive agents on the electrochemical performance of SiO₂ gel anode were systematically investigated and compared. The results show that KB provides far better cycling and rate performance than SP and AB for SiO₂ anode electrodes, with a reversible specific capacity of 351.4 mA h g^{−1} at 0.2 A g^{−1} after 200 cycles and a stable 311.7 mA h g^{−1} at 1.0 A g^{−1} after 500 cycles. The enhanced mechanism of the lithium storage performance of SiO₂-KB anode was also proposed.

Keywords: silica-based anode; Ketjen Black; electrochemical properties; lithium-ion battery



Citation: Hu, G.; Sun, X.; Liu, H.; Xu, Y.; Liao, L.; Guo, D.; Liu, X.; Qin, A. Improvement of Lithium Storage Performance of Silica Anode by Using Ketjen Black as Functional Conductive Agent. *Nanomaterials* **2022**, *12*, 692. <https://doi.org/10.3390/nano12040692>

Academic Editors: Xiang Wu and Jung Woo Lee

Received: 16 January 2022

Accepted: 8 February 2022

Published: 19 February 2022

Publisher's Note: MDPI stays neutral with regard to jurisdictional claims in published maps and institutional affiliations.



Copyright: © 2022 by the authors. Licensee MDPI, Basel, Switzerland. This article is an open access article distributed under the terms and conditions of the Creative Commons Attribution (CC BY) license (<https://creativecommons.org/licenses/by/4.0/>).

1. Introduction

Lithium-ion batteries (LIBs) have attracted much attention due to their high energy density and long cycle life. To meet the demand for scaled-up LIBs, the development of electrode materials with high performance is necessary. Graphite is widely used as anode material for LIBs [1], however, its theoretical lithium storage capacity is relatively low, only 372 mA h g^{−1}. Therefore, silicon-based anode materials with higher theoretical specific capacity (4200 mA h g^{−1}) are considered to be anode materials for next-generation LIBs [2–4]. However, the severe volume expansion (>300%) associated with the various phase transitions during the intercalation and escape of lithium in/out Si particles have been a major disadvantage, as this led to rapid capacity fading and significantly limited commercial application [5]. Although novel silicon anodes with nanosphere [6,7], nanotube [8,9], core-shell structure [10,11] and other new structures could improve the cycling performance [12,13], the complicated process and expensive preparation technology are prohibitive. In addition, the low initial coulombic efficiency and the poor conductivity also limited its application [14–16]. Compared to elemental Si anode, silicon oxides show a smaller volume change during cycling. Furthermore, when using silicon oxides as anodes, the in situ generated Li₂O and lithium silicates during the first lithiation may buffer the large volume change and lead to the improvement of cycling stability. In cutting-edge researches, silica [17] with hollow [18], porous [19,20], and other special structures were composited with carbon [19,21,22], graphite [23], metal [24], and metal oxides [25–28] to improve its conductivity and lithium storage performance. These methods could effectively improve the electrochemical performance of silica anodes.

Carbon conductive agents, which were added during the electrode manufacturing process, played an important role in the impedance and electrode density. However, their functional mechanism still needs further investigation [29,30]. The literature has reported that conductive agents could be used as the mediator [31] to form a conductive network in electrodes, reducing the contact resistance of the electrode and improving the electron transport rate. Commercial carbon black, such as acetylene black (AB) and Super-P (SP), have been used as conductive agents in LIBs [32,33]. Compared with AB and SP, Ketjen Black (KB) has the advantages of large specific surface area, excellent electrical conductivity, and relatively narrow pore size distribution, when used as the conductive agent [34]. However, the systematic study of the effect of KB on silica anodes is sparsely reported.

Herein, a network nanostructure of silica (SiO_2) anode material using KB as a conductive agent with high electrochemical performance was prepared. The effects of KB on the electrochemical performance of silica anode materials were systematically studied. Furthermore, the enhanced storage mechanism of the SiO_2 -KB anode materials was proposed. This work revealed that the type of conductive agent played a key role on the electrochemical performance of anode materials.

2. Materials and Methods

2.1. Synthesis

Briefly, SiO_2 aerogels were prepared by the sol-gel method [35]. It was obtained by taking 8 mL of anhydrous ethanol in a beaker, adding ammonia to adjust the pH to 9–10, then slowly adding 0.5 mL of TEOS, and left for 4 h at room temperature before adding 1 mL of deionized water to prepare the gel, and freeze-drying to obtain SiO_2 aerogels.

SiO_2 nanospheres were obtained by first taking 3 mL of $\text{NH}_3 \cdot \text{H}_2\text{O}$ and 60 mL of alcohol to be mixed and stirred thoroughly, then 1.5 mL of TEOS was added into the above solution and continued stirring for 10 h at room temperature to obtain a white emulsion, finally the solid product was collected by centrifugation, washed several times with distilled water and alcohol, and dried at 70 °C for 12 h in a vacuum.

2.2. Materials Characterization

Morphological and compositional analyses for the as-prepared sample were performed with Transmission Electron Microscope (TEM, JEM-2100F, JEOL Inc., Tokyo, Japan) and field emission scanning electron microscopy (SEM, S-4800, HITACHI Inc., Tokyo, Japan), respectively, the crystallographic structure of the obtained SiO_2 were characterized by X-ray diffraction (XRD, X' Pert PRO, PANalytical Inc., Almelo, The Netherlands), the chemical component of the SiO_2 anode was investigated using an X-ray photoelectron spectroscope (XPS, ESCALAB 250Xi, Thermo Fisher Scientific Inc., Waltham, MA, USA) using Al $\text{K}\alpha$ radiation, the electrical resistance and electrical resistivity were tested by four-point probe meter (FPM, RTS-2A, 4 PROBES TECH Inc., China).

2.3. Electrochemical Measurements

The working electrodes were fabricated by compressing a mixture of the active materials (SiO_2 nanospheres), a conductive material of KB, AB, or SP, and a binder of polyvinylidene fluoride at the mass ratio of 50:30:20 onto Cu foil current collector (10 μm in thickness), then dried at 110 °C for 12 h. 0.1 mL of 1 M LiPF_6 in EC/DMC/DEC (Ethylene carbonate/Dimethyl carbonate/Diethyl carbonate) with volume ratio of 1:1:1 was used as the electrolyte, electrochemical experiments of half cells were carried out in CR2025 coin-type cells, 0.6 mm thick lithium discs are used as counter electrodes, and Polypropylene diaphragm type Celgard 2500 as battery separator. The cells were assembled in an argon-filled glove box (MIKROUNA, LAB2000, Shanghai, China). The specific capacity was measured by a galvanostatic discharge-charge method in the voltage range between 3.0 V and 0.01 V at a current density of 100 mA g^{-1} with SiO_2 as the active material mass on a battery test system (Neware, BTS 5 V 10 mA, Shenzhen, China). Cyclic voltammetry was performed

using an electrochemical workstation (CV, CHI 690D, CH Instruments Ins, Wuhan, China) between 3 V and 0.01 V (vs. Li/Li⁺) at a scan rate of 0.5 mV s⁻¹.

3. Results and Discussion

Figure 1a shows the SEM image of the SiO₂ aerogel, and it can be seen that the prepared SiO₂ aerogel particles are uniform in size with sphere in shape. Figure 1b shows that the average size of SiO₂ aerogel particle is about 100 nm. Figure 1c is the XRD pattern of the SiO₂ aerogel, the crystal structure of the prepared silica aerogel only shows a broad diffraction peak at around 23°, indicating an amorphous structure.

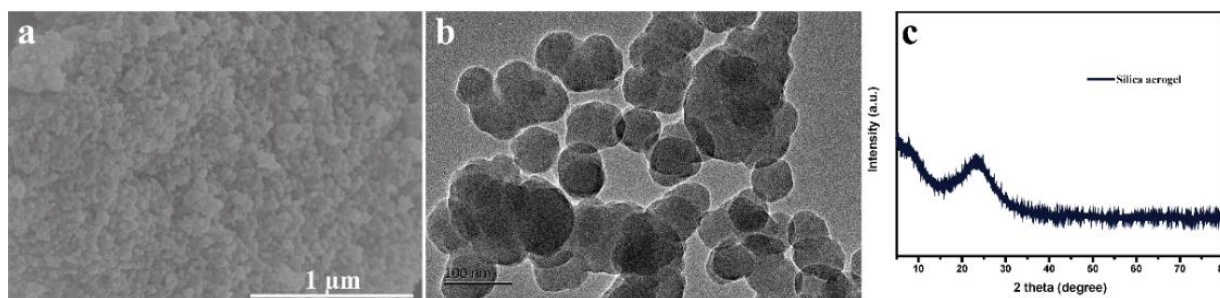


Figure 1. SEM (a), TEM (b) image, and XRD (c) pattern of silica aerogel.

Figure 2 shows the TEM and elemental mapping images of SiO₂ aerogel mixed with different conductive agents, respectively. It can be seen that different conductive agents form different structures when combined with silica aerogel. Figure 2a shows that the aerogel mixture with KB (SiO₂-KB) has an internet structure with uniformly dispersed nanoparticles, which indicates that a conductive network can be formed to provide a large number of effective conductive pathways and contacts for Li-ions. Furthermore, the elemental distribution shows a cobweb-like carbon chain pathway. For comparison, we also investigated the differences in the composition of the conductive pathways of SiO₂-SP and SiO₂-AB, respectively, under identical conditions. Figure 2b shows that the SiO₂-SP has a branched structure with larger SiO₂ particles and more agglomerates than that of SiO₂-KB. Figure 2c shows that the SiO₂-AB stacks together and has more agglomerate structure than that of SiO₂-SP and SiO₂-KB. Therefore, it is clear that the SiO₂-KB has the best dispersion, indicating it has excellent conductive network channels.

To further confirm the effects of the three conductive agents on the electrochemical performance of SiO₂ anode, a four-probe electrical resistance test was carried out and the result is shown in Table 1, the type of conductive agents plays an important role on the electrical resistance of SiO₂ anode. KB provides much lower electrical resistance and electrical resistivity than SP and AB for SiO₂ anode, which is helpful to improve the rate performance of electrode.

Table 1. The electrical resistance and electrical resistivity of anode electrodes.

Sample	SP	AB	KB
sheet resistance (Ω)	125.0	148.2	64.9
electrical resistivity (Ω·cm)	12.50	14.82	6.49

The cycling performance and coulombic efficiency of the SiO₂ anode with different conductive agents are shown in Figure 3a. The first discharge capacity of SiO₂-KB reaches 378.2 mA h g⁻¹, the capacity has a slight decrease in the several consequent cycles, and maintains 351.4 mA h g⁻¹ after 200th cycles at 0.2 A g⁻¹. In comparison to SiO₂-KB, electrodes of SiO₂-SP and SiO₂-AB exhibit a lower reversible capacity of 139.4 mA h g⁻¹ and 118.7 mA h g⁻¹ at the first cycle and after 100th cycles display the

capacity of $163.9 \text{ mA h g}^{-1}$ and $137.7 \text{ mA h g}^{-1}$ at 0.2 A g^{-1} , respectively, which indicates that KB is more beneficial in facilitating the silica electrochemical reaction. The specific capacity of $\text{SiO}_2\text{-KB}$ decreased before the first 40 cycles, and then gradually increased, even after more than 100 cycles; the former is mainly due to the gradual lithiation of SiO_2 and the generated irreversible products such as lithium silicate and Li_2O , and the latter is due to the generated elemental silicon, which can provide the reversible specific capacity by the Si-Li alloy reaction.

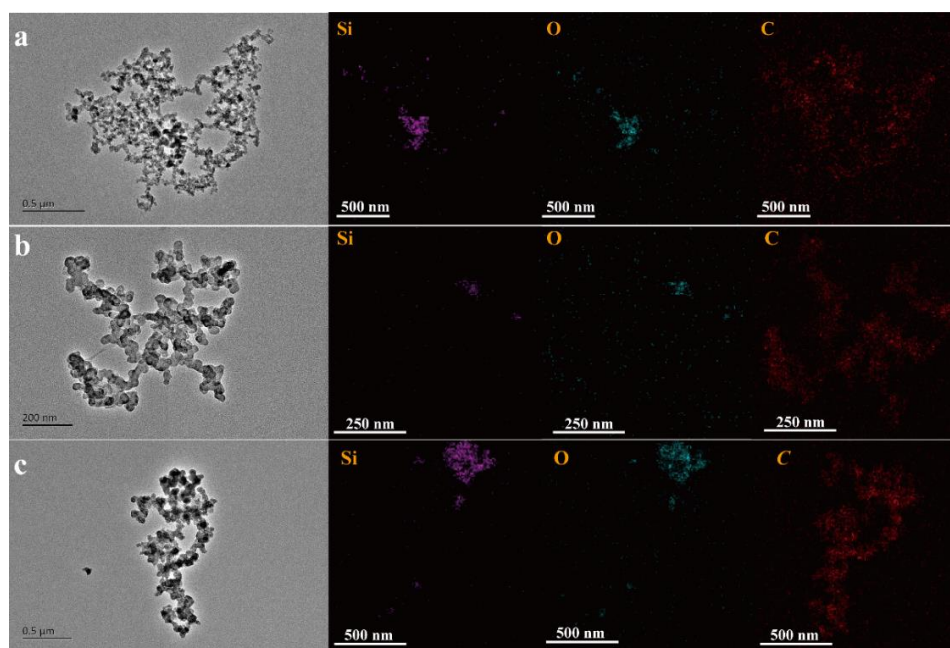


Figure 2. TEM and elemental mapping images of silica aerogels mixed with KB (a), SP (b), and AB (c).

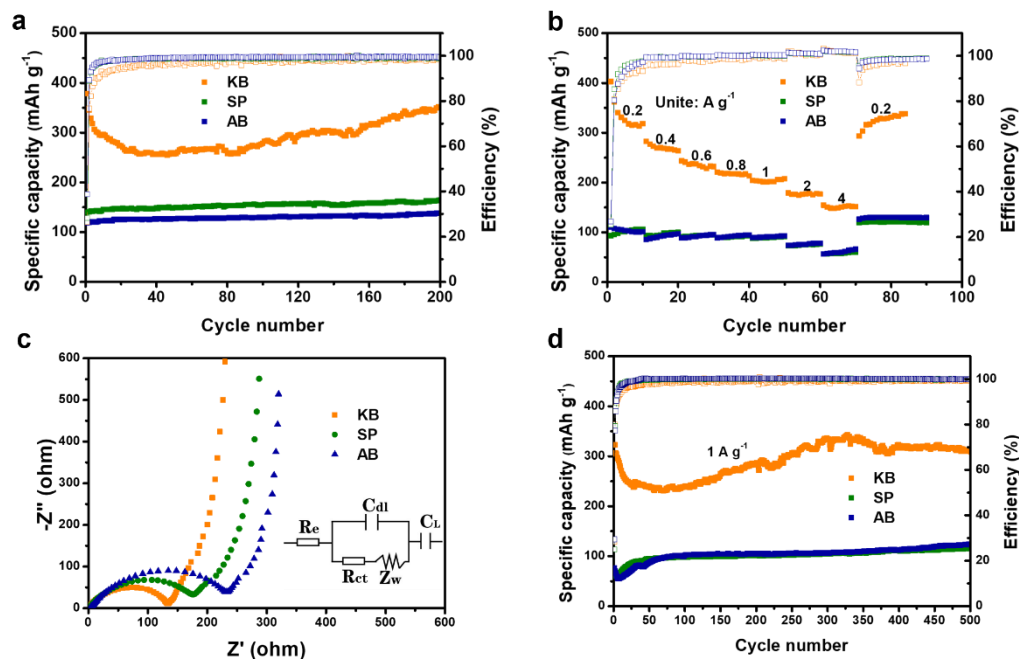


Figure 3. Cycle performance with coulombic efficiency at a current density of 200 mA g^{-1} (a), Rate capability at various current densities (b), Nyquist plot (c), and long-term cycling performance at a current density of 1.0 A g^{-1} (d) of silica aerogel anode with three carbon conductive agent.

The rate capability of the electrodes is shown in Figure 3b, with different current densities of 0.2, 0.4, 0.6, 0.8, 1.0, 2.0, and 4.0 A g⁻¹. The SiO₂-KB electrode attains an average discharge capacity of 318.2 mA h g⁻¹, 263.6 mA h g⁻¹, 231.9 mA h g⁻¹, 213.4 mA h g⁻¹, 207.7 mA h g⁻¹, 176.7 mA h g⁻¹, and 151.4 mA h g⁻¹, respectively, at the above current densities. The stable high reversible capacity of 331.1 mA h g⁻¹ recovered when the current density turned back to 0.2 A g⁻¹. Compared to SiO₂-SP and SiO₂-AB, SiO₂-KB shows more excellent rate properties, indicating that the SiO₂-KB has excellent structural stability.

To determine the origin of the electrochemical behavior of SiO₂-KB, electrochemical impedance spectra (EIS) test was performed at their open-circuit potential. The equivalent circuits inserted in Figure 3c were employed to analyze the Nyquist plot of the desired anode material. The total impedance could be regarded as the electrolyte resistance R_e and the charge transfer resistance R_{ct} , and C_{dl} is the double-layer capacitance. Z_w is the Warburg impedance that reflects the diffusion of lithium-ion in the solid. C_L means the simplified intercalation capacitance. A semicircle was an indication for the charge transfer at high frequency range, while the straight line for the low frequency lithium-ion diffusion in the electrode material [36]. Obviously, the resistance of SiO₂-KB ($R_{ct} = 130 \Omega$) is much lower than that of SiO₂-SP ($R_{ct} = 180 \Omega$) and SiO₂-AB ($R_{ct} = 240 \Omega$), suggesting that KB could remarkably enhance the silica electrical conductivity. Furthermore, SiO₂-KB presents an exciting long-term cycling performance and delivers a specific capacity of 311.7 mA h g⁻¹ at a current density of 1.0 A g⁻¹ after 500 cycles. In comparison to SiO₂-KB, SiO₂-SP and SiO₂-AB exhibit a much lower reversible capacity of 66.4 mA h g⁻¹ and 75.9 mA h g⁻¹, respectively, at the first cycle, and after 500th cycles, the capacity only remains 115.5 mA h g⁻¹ and 123.9 mA h g⁻¹, respectively, which is shown in Figure 3d.

To confirm the structural integrity of the electrodes after cycle tests, SEM images of the different electrodes with the three conductive agents after 200 cycles were obtained and illustrated in Figure 4. For the electrode of SiO₂-KB, the shape of SiO₂ remained constant after 200 cycles (Figure 4a,b). For the electrode of SiO₂-SP, the silica undergoes a slight agglomeration phenomenon after 200 cycles (Figure 4c,d), while for the electrode of SiO₂-AB, the SiO₂ particles stick together and form large particles after 200 cycles (Figure 4e,f), which reduces the contact area between the silica, and leads to the reduction in capacity.

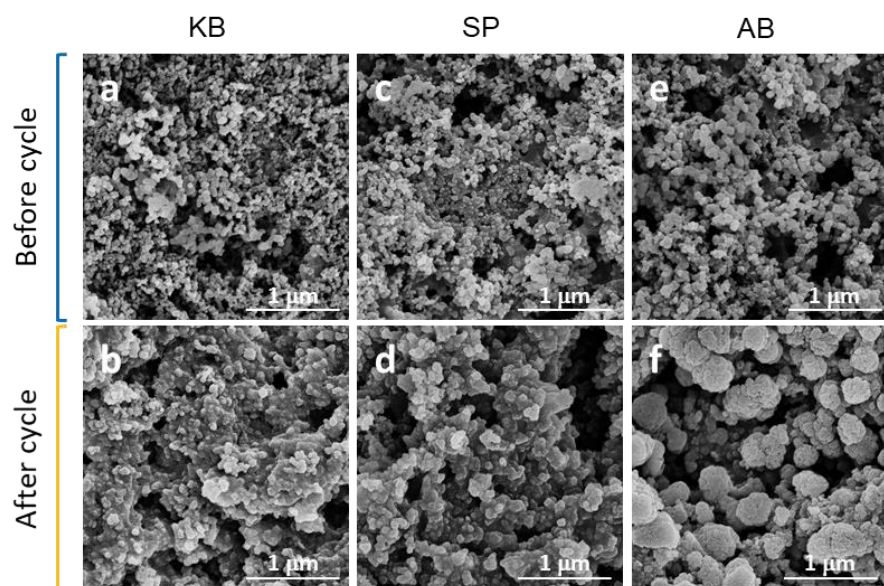


Figure 4. SEM images of SiO₂ electrode with KB (a,b), SP (c,d), and AB (e,f) before and after 200 cycles.

Figure 5 shows the CV curves of the SiO₂ aerogel electrodes at a scan rate of 0.5 mV s⁻¹ with three different conductive agents, respectively. As can be seen in Figure 5, the reduction characteristic peak potential for the reaction of silica to produce lithium silicate and lithium oxide is 0.42 V, 0.65 V, and 0.8 V when using KB, SP, and AB as the conductive agent,

respectively. The peak potential is significantly shifted to a smaller voltage for the KB (Figure 5a) compared to the SP (Figure 5b) and AB (Figure 5c). The oxidation characteristic peak potential of 0.25 V for the silicon-lithium alloy when using KB as the conductive agent also shows a significant shift to a smaller voltage compared to the SP (0.28 V) and AB (0.35 V), which is mainly due to the fact that KB has higher conductivity than SP and AB, where KB acts as a microcurrent collector between SiO₂ and the current collector to accelerate the speed of electron movement and also effectively increase the migration rate of Li⁺ in the electrode material. Subsequently, the polarization of the silica anode is reduced, which will facilitate the occurrence of electrochemical reactions [37].

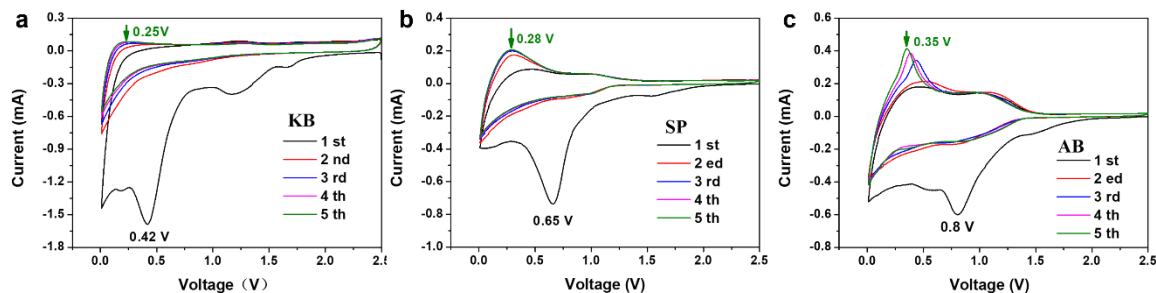


Figure 5. CV curve for the first five cycles of the silica aerogel when KB (a), SP (b), and AB (c) as conductive agents.

The chemical states of Si in SiO₂ anode with KB (Figure 6a), SP (Figure 6b) and AB (Figure 6c) during discharge/charge were identified by XPS, where energy correction for surface contamination was performed using C1s (284.6 eV) as a standard. The Si 2p_{3/2} peak shifts from 104.0 to 103.0 eV when discharged to 0.01 V, suggesting the reduction in Si to Li_xSi. When charged to 3 V, the peak shifts back to the original position of the SiO₂ electrode before discharge/charge (blue curve). It is clear that the curve in SiO₂-KB fluctuates more strongly than the smooth curves in SiO₂-SP and SiO₂-AB, indicating that the electrochemical reaction promoted by SiO₂ using KB as a conductive agent produces a higher amount of products containing elemental silicon, which is conducive to the improvement of electrochemical performance.

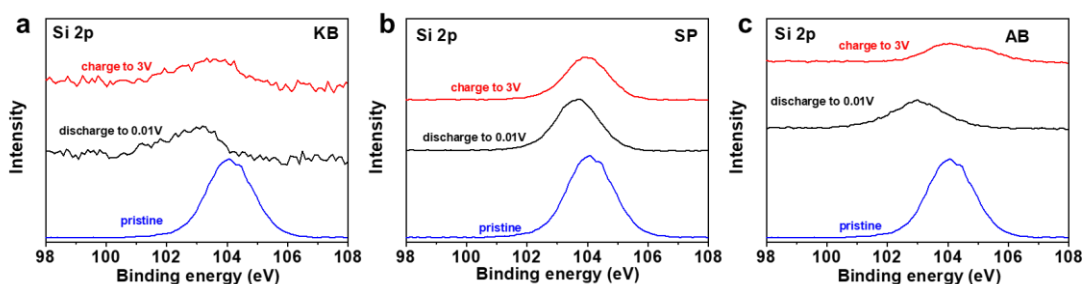
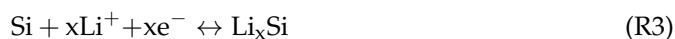
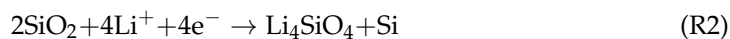


Figure 6. Si 2p XPS spectra of SiO₂ anode with KB (a), SP (b) and AB (c) at different states.

Based on previous researches, the possible electrochemical reaction mechanisms of SiO₂ can be summarized into the following reactions [38,39]:



Reactions of R1, and R2 are irreversible (potential of KB-0.25 V, SP-0.28 V, AB-0.35 V) and occur simultaneously although they compete with each other, and the obtained Si is

electrochemically active, while Li_2O , and Li_4SiO_4 are electrochemically inactive [22]. The reaction R1 can produce more Si and result in a higher capacity than the reaction R2 [13].

To better understand the storage mechanism and excellent high-rate performance of the SiO_2 aerogel electrode with KB, the CV curves of the SiO_2 aerogel electrode under the three carbon conductive agents at different scan rates from 0.5 to 5 mV s^{-1} were collected and shown in Figure 7a,e,i. Generally, the current obeys a function relationship with the voltage during the sweep [40–43]:

$$i = av^b \quad (1)$$

where a and b are the parameters. The capacity contributions from the diffusion-controlled intercalation process and the surface-induced capacitive process can be qualitatively analyzed by the b -value. For a diffusion-controlled process, the b -value is 0.5, while the b -value near 1 means a totally capacitive-controlled process. According to the fitted line $\log(v)$ - $\log(i)$ curve depicted in Figure 7b,f,j, the b -value is 0.84, 0.86, 0.66, respectively. Furthermore, in view of the capacity contribution, the current (i) under a certain potential (V) can be divided into two parts [42–44]:

$$i(V) = k_1v + k_2v^{\frac{1}{2}} \quad (2)$$

where k_1v and $k_2v^{\frac{1}{2}}$ present charge stemmed from the surface capacitive charge and diffusion-controlled charge, respectively. The area share of the pseudocapacitive behavior of the silica aerogel electrodes with the three different conductive agents is shown in the paler parts of Figure 7c,g,k. The pseudocapacitance contributions are shown in Figure 7d,h,l. The pseudocapacitance contribution of the SiO_2 aerogel electrode with KB at scan rates of 1.0 to 5.0 mV s^{-1} is 41%, 49%, 54%, 58% and 61%, respectively; 51%, 58%, 63%, 67% and 70%, respectively, for SP and 65%, 73%, 77%, 79% and 80%, respectively, for AB. It can be seen that the use of different forms of conductive agents has a greater effect on the contribution of the pseudocapacitance in the SiO_2 aerogel electrode. The storage mechanism of the SiO_2 -KB electrode is dominated by diffusion-controlled intercalation behavior, which is due to the excellent conductive network structure of KB and leads to an accelerated redox reaction. The contribution of surface-driven pseudocapacitance behavior for the SiO_2 -KB electrode gradually increases as the scan rate increases, but is still less than that SiO_2 -SP and SiO_2 -AB. The contribution of the pseudocapacitance behavior of the SiO_2 -KB electrode increases with increasing scan rate, however remains smaller than that of the SiO_2 -SP and SiO_2 -AB electrodes.

Li^+ diffusion coefficients during electrochemical charge/discharge for silica aerogels with different conductive agents calculated from the GITT method [45–47] are presented in Figure 8. The voltage change curve of the first charge/discharge under pulse current when using three different carbon conductive agents is shown in Figure 8a, and the Li^+ diffusion coefficient calculated from the pulse charge/discharge curve is shown in Figure 8b. The longer charging and discharging duration of Li^+ in the diffusivity test curve of SiO_2 -KB is due to the special network structure of KB, which enables the nano- SiO_2 particles to perform electrochemical reactions without agglomeration and less hindering to the transport of Li^+ . This indicates that the KB conductive agent accelerates the diffusion of Li^+ and enables the sufficient electrochemical reaction of SiO_2 [16].

In order to confirm the effect of the KB, the electrochemical properties of SiO_2 nanosphere anode was compared with three different conductive agents, respectively. The morphology of the SiO_2 nanospheres is shown in Figure 9a, which has a nice monodispersity and smooth surface with an average particle size of 100 nm. The inset in Figure 9a shows the XRD pattern of the SiO_2 nanospheres; a broad peak at 23° suggesting that the SiO_2 nanospheres are amorphous in structure similar to the SiO_2 aerogels. Figure 9b–d show the CV curves of the SiO_2 nanosphere anode at a scan rate of 0.5 mV s^{-1} when using the three different conductive agents, respectively. The reduction characteristic peak potential for the reaction of SiO_2 to produce Li_2O and Li_4SiO_4 locates at 0.5 V for the SiO_2 nanospheres-KB anode, which has a significant shift to the left compared to the anodes of SiO_2 nanospheres-SP (0.85 V) and SiO_2 nanospheres-AB (0.9 V), indicating that it also has the similar effect of reducing polarization

of SiO₂ anodes prepared by different methods when using KB as the conducting agent, and strongly promotes the electrochemical reaction.

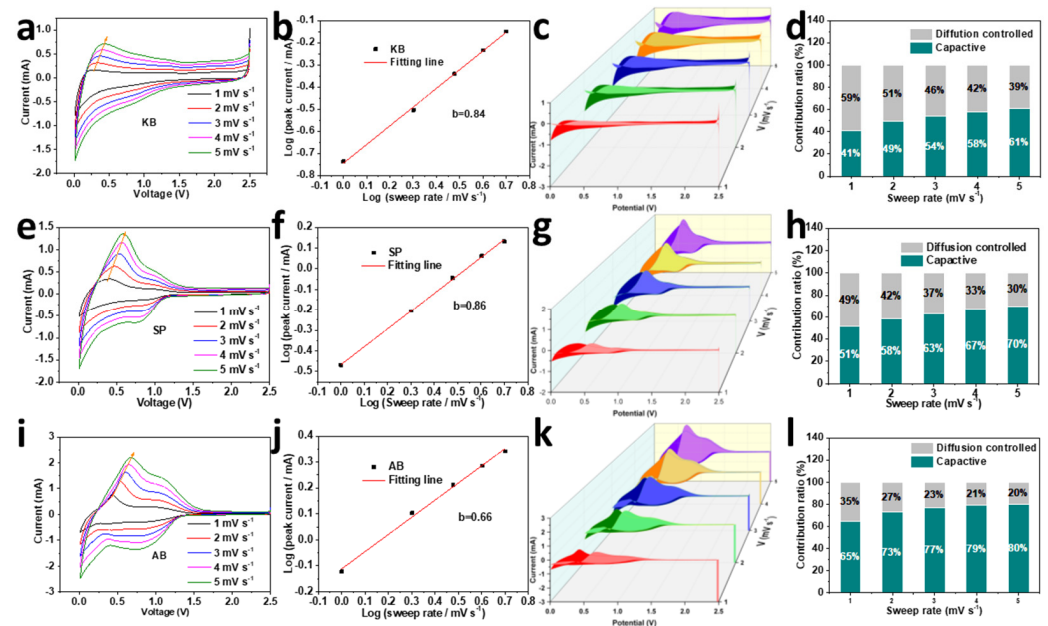


Figure 7. Behaviors of pseudocapacitance in silica aerogels using KB (a–d), SP (e–h), and AB (i–l) as conductive agents.

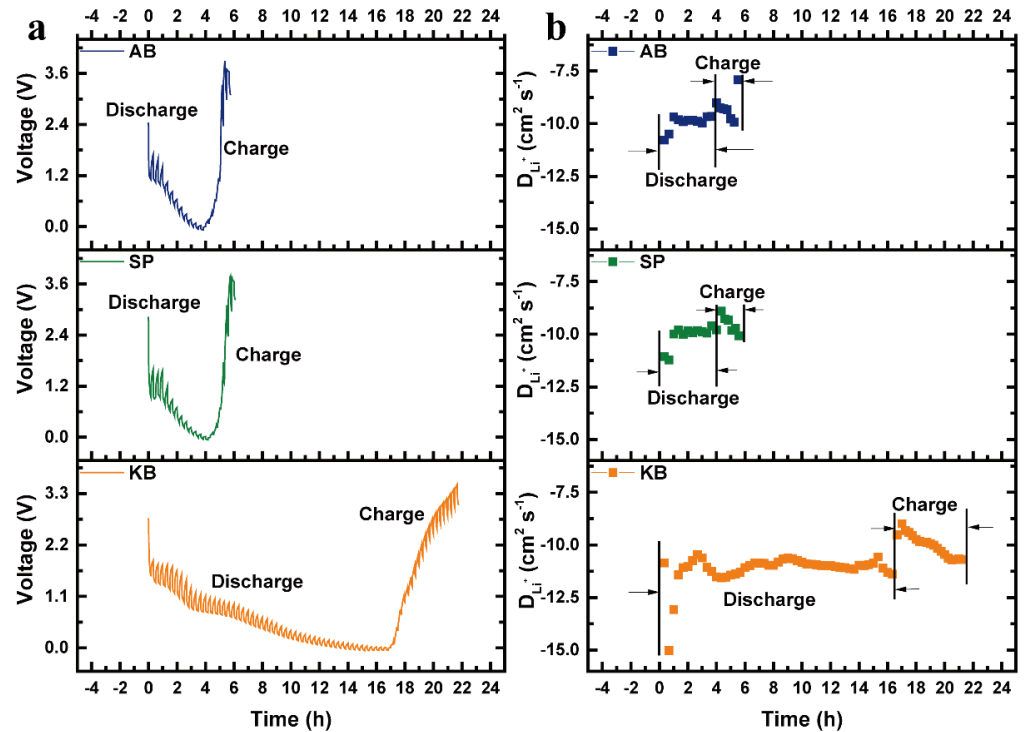


Figure 8. The voltage change curve of the first charge/discharge under pulse current (a) and Li-ion diffusion coefficient calculated from the pulse charge/discharge curve (b) with different carbon conductive agents.

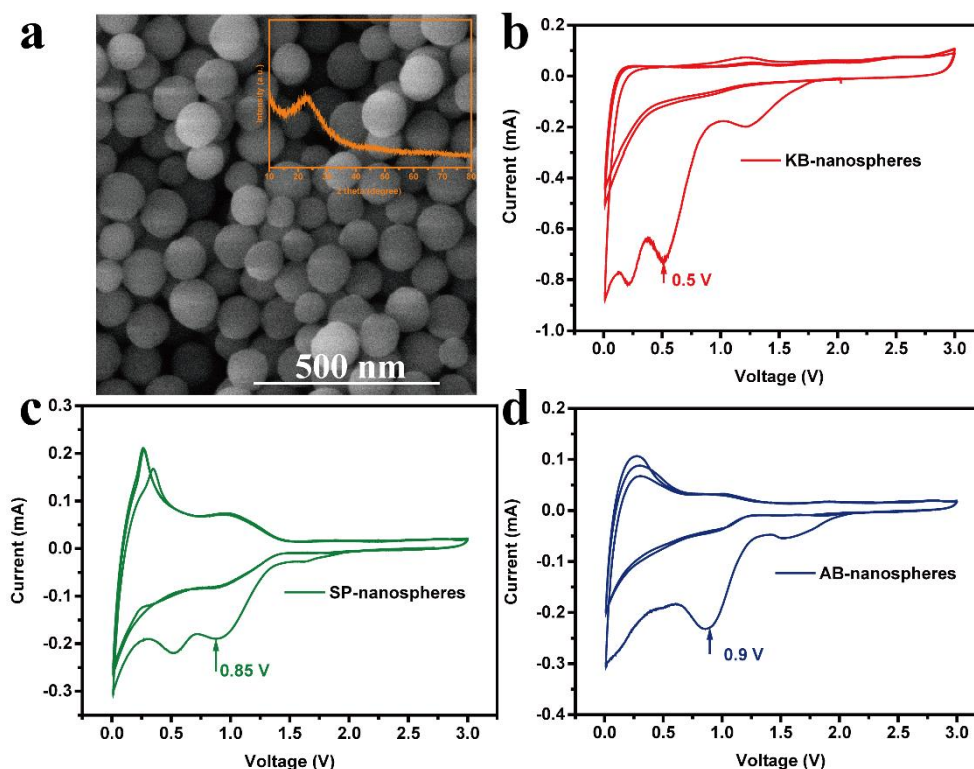


Figure 9. The SEM image and XRD pattern (the inset) (a) of silica nanospheres, CV curves of the first three cycles of the silica nanospheres when using KB (b), SP (c), and AB (d) as conductive agents, respectively.

The function of KB can be described as a schematic diagram conductive network, as shown in Figure 10, the special structure of KB connects the SiO₂ aerogel particles together and forms an excellent conductive network of dispersed SiO₂-KB, which provides rich electron transfer channels and improves the electrochemical performance of silica anode.

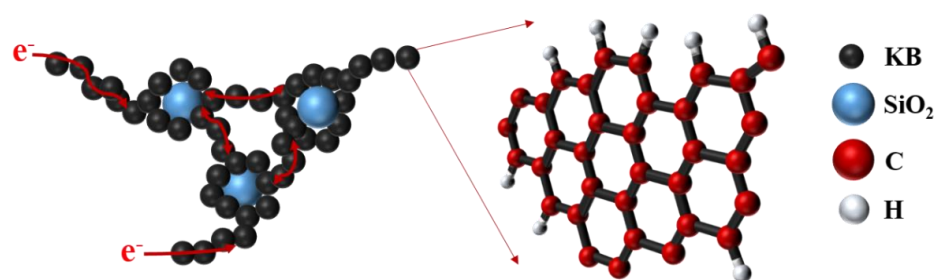


Figure 10. Schematic diagram conductive network of KB.

4. Conclusions

In summary, the effects of the types and the structures of conductive agents on the electrochemical performance of SiO₂ aerogel electrode were investigated, and the results show that the KB as a conductive agent not only can uniformly disperse and wrap the SiO₂ nanoparticles, but also can build a good conductive network to enhance the transport rate of lithium-ions and effectively increase their electrochemical activity. This work proves and verifies that SiO₂ aerogel can be used as a recommended electrode material for high-rate LIBs through choosing appropriate conductive agent.

Author Contributions: Conceptualization, methodology, writing—original draft preparation, investigation, and resources, G.H.; data curation, visualization, X.S.; software, H.L.; validation, D.G.,

L.L. and X.L.; formal analysis, Y.X.; writing—review and editing, supervision, project administration, and funding acquisition, A.Q.; All authors have read and agreed to the published version of the manuscript.

Funding: This work was supported by the Natural Science Foundation of Guangxi province (2018JJA160029, 2018GXNSFAA138041), the Foundation of Guangxi Key Laboratory of Optical and Electronic Materials and Devices (20AA-17), and Innovation Project of Guangxi Graduate Education (YCSW2021199, YCBZ2021062).

Institutional Review Board Statement: Not applicable.

Informed Consent Statement: Not applicable.

Data Availability Statement: The data presented in this study are available from the corresponding author upon request.

Acknowledgments: We acknowledge the support of the Key Laboratory of New Processing Technology for Non-ferrous Metals and Materials of the Ministry of Education, School of Materials Science and Engineering, Guilin University of Technology.

Conflicts of Interest: The authors declare no conflict of interest.

References

1. Zhang, Z.; Wang, F.; An, Q.; Li, W.; Wu, P. Synthesis of graphene@Fe₃O₄@C core-shell nanosheets for high-performance lithium ion batteries. *J. Mater. Chem. A* **2015**, *3*, 7036–7043. [[CrossRef](#)]
2. Hou, G.; Cheng, B.; Yang, Y.; Du, Y.; Zhang, Y.; Li, B.; He, J.; Zhou, Y.; Yi, D.; Zhao, N.; et al. Multiscale Buffering Engineering in Silicon–Carbon Anode for Ultrastable Li-Ion Storage. *ACS Nano* **2019**, *13*, 10179–10190. [[CrossRef](#)]
3. Choi, J.W.; Aurbach, D. Promise and reality of post-lithium-ion batteries with high energy densities. *Nat. Rev. Mater.* **2016**, *1*, 16013. [[CrossRef](#)]
4. Tu, J.; Yuan, Y.; Zhan, P.; Jiao, H.; Wang, X.; Zhu, H.; Jiao, S. Straightforward Approach toward SiO₂ Nanospheres and Their Superior Lithium Storage Performance. *J. Phys. Chem. C* **2014**, *118*, 7357–7362. [[CrossRef](#)]
5. Song, T.; Xia, J.; Lee, J.-H.; Lee, D.H.; Kwon, M.-S.; Choi, J.-M.; Wu, J.; Doo, S.K.; Chang, H.; Park, W.I.; et al. Arrays of Sealed Silicon Nanotubes As Anodes for Lithium Ion Batteries. *Nano Lett.* **2010**, *10*, 1710–1716. [[CrossRef](#)] [[PubMed](#)]
6. Li, J.Y.; Li, G.; Zhang, J.; Yin, Y.X.; Yue, F.S.; Xu, Q.; Guo, Y.G. Rational Design of Robust Si/C Microspheres for High-Tap-Density Anode Materials. *ACS Appl. Mater. Interfaces* **2019**, *11*, 4057–4064. [[CrossRef](#)]
7. Xu, Q.; Li, J.Y.; Sun, J.K.; Yin, Y.X.; Wan, L.J.; Guo, Y.G. Watermelon-Inspired Si/C Microspheres with Hierarchical Buffer Structures for Densely Compacted Lithium-Ion Battery Anodes. *Adv. Energy Mater.* **2017**, *7*, 1601481. [[CrossRef](#)]
8. Ma, T.; Xu, H.; Yu, X.; Li, H.; Zhang, W.; Cheng, X.; Zhu, W.; Qiu, X. Lithiation Behavior of Coaxial Hollow Nanocables of Carbon–Silicon Composite. *ACS Nano* **2019**, *13*, 2274–2280. [[CrossRef](#)]
9. Zhang, C.; Gu, L.; Kaskhedikar, N.; Cui, G.; Maier, J. Preparation of Silicon@Silicon Oxide Core–Shell Nanowires from a Silica Precursor toward a High Energy Density Li-Ion Battery Anode. *ACS Appl. Mater. Interfaces* **2013**, *5*, 12340–12345. [[CrossRef](#)]
10. Zhai, W.; Ai, Q.; Chen, L.; Wei, S.; Li, D.; Zhang, L.; Si, P.; Feng, J.; Ci, L. Walnut-inspired micro-sized porous silicon/graphene core-shell composites for high-performance lithium-ion battery anodes. *Nano Res.* **2017**, *10*, 4274–4283. [[CrossRef](#)]
11. Lu, B.; Ma, B.; Deng, X.; Li, W.; Wu, Z.; Shu, H.; Wang, X. Cornlike Ordered Mesoporous Silicon Particles Modified by Nitrogen-Doped Carbon Layer for the Application of Li-Ion Battery. *ACS Appl. Mater. Interfaces* **2017**, *9*, 32829–32839. [[CrossRef](#)] [[PubMed](#)]
12. Chen, X.; Li, X.; Ding, F.; Xu, W.; Xiao, J.; Cao, Y.; Meduri, P.; Liu, J.; Graff, G.L.; Zhang, J.-G. Conductive Rigid Skeleton Supported Silicon as High-Performance Li-Ion Battery Anodes. *Nano Lett.* **2012**, *12*, 4124–4130. [[CrossRef](#)]
13. Gowda, S.R.; Pushparaj, V.; Herle, S.; Girishkumar, G.; Gordon, J.G.; Gullapalli, H.; Zhao, X.; Ajayan, P.M.; Reddy, A.L.M. Three-dimensionally engineered porous silicon electrodes for Li ion batteries. *Nano Lett.* **2012**, *12*, 6060–6065. [[CrossRef](#)] [[PubMed](#)]
14. Liu, Z.; Yu, Q.; Zhao, Y.; He, R.; Xu, M.; Feng, S.; Li, S.; Zhou, L.; Mai, L. Silicon oxides: A promising family of anode materials for lithium-ion batteries. *Chem. Soc. Rev.* **2018**, *48*, 285–309. [[CrossRef](#)]
15. Liang, C.; Zhou, L.; Zhou, C.; Huang, H.; Liang, S.; Xia, Y.; Gan, Y.; Tao, X.; Zhang, J.; Zhang, W. Submicron silica as high-capacity lithium storage material with superior cycling performance. *Mater. Res. Bull.* **2017**, *96*, 347–353. [[CrossRef](#)]
16. Zhang, Y.; Li, Y.; Wang, Z.; Zhao, K. Lithiation of SiO₂ in Li-Ion Batteries: In Situ Transmission Electron Microscopy Experiments and Theoretical Studies. *Nano Lett.* **2014**, *14*, 7161–7170. [[CrossRef](#)]
17. Chang, W.S.; Park, C.M.; Kim, J.H.; Kim, Y.U.; Jeong, G.; Sohn, H.J. Quartz (SiO₂): A new energy storage anode material for Li-ion batteries. *Energy Environ. Sci.* **2012**, *5*, 6895–6899. [[CrossRef](#)]
18. Ma, X.; Wei, Z.; Han, H.; Wang, X.; Cui, K.; Yang, L. Tunable construction of multi-shell hollow SiO₂ microspheres with hierarchically porous structure as high-performance anodes for lithium-ion batteries. *Chem. Eng. J.* **2017**, *323*, 252–259. [[CrossRef](#)]

19. Yuan, Z.; Zhao, N.; Shi, C.; Liu, E.; He, C.; He, F. Synthesis of SiO₂/3D porous carbon composite as anode material with enhanced lithium storage performance. *Chem. Phys. Lett.* **2016**, *651*, 19–23. [[CrossRef](#)]
20. Li, H.H.; Wu, X.L.; Sun, H.Z.; Wang, K.; Fan, C.Y.; Zhang, L.L.; Yang, F.M.; Zhang, J.P. Dual-Porosity SiO₂/C Nanocomposite with Enhanced Lithium Storage Performance. *J. Phys. Chem. C* **2015**, *119*, 3495–3501. [[CrossRef](#)]
21. Xiao, T.; Zhang, W.; Xu, T.; Wu, J.; Wei, M. Hollow SiO₂ microspheres coated with nitrogen doped carbon layer as an anode for high performance lithium-ion batteries. *Electrochim. Acta* **2019**, *306*, 106–112. [[CrossRef](#)]
22. Liu, X.; Chen, Y.; Liu, H.; Liu, Z.-Q. SiO₂@C hollow sphere anodes for lithium-ion batteries. *J. Mater. Sci. Technol.* **2017**, *33*, 239–245. [[CrossRef](#)]
23. Li, H.H.; Zhang, L.L.; Fan, C.Y.; Wang, K.; Wu, X.L.; Sun, H.Z.; Zhang, J.P. A plum-pudding like mesoporous SiO₂/flake graphite nanocomposite with superior rate performance for LIB anode materials. *Phys. Chem. Chem. Phys.* **2015**, *17*, 22893–22899. [[CrossRef](#)]
24. Tang, C.; Liu, Y.; Xu, C.; Zhu, J.; Wei, X.; Zhou, L.; He, L.; Yang, W.; Mai, L. Ultrafine Nickel-Nanoparticle-Enabled SiO₂ Hierarchical Hollow Spheres for High-Performance Lithium Storage. *Adv. Funct. Mater.* **2017**, *28*, 1704561. [[CrossRef](#)]
25. Hou, Y.; Yuan, H.; Chen, H.; Shen, J.; Li, L. The preparation and lithium battery performance of core-shell SiO₂@Fe₃O₄@C composite. *Ceram. Int.* **2017**, *43*, 11505–11510. [[CrossRef](#)]
26. Tian, Q.; Chen, Y.; Chen, F.; Zhang, W.; Chen, J.; Yang, L. Etching-free template synthesis of double-shelled hollow SiO₂@SnO₂@C composite as high performance lithium-ion battery anode. *J. Alloy. Compd.* **2019**, *809*, 151793. [[CrossRef](#)]
27. Liu, F.; Chen, Z.; Fang, G.; Wang, Z.; Cai, Y.; Tang, B.; Zhou, J.; Liang, S. V₂O₅ Nanospheres with Mixed Vanadium Valences as High Electrochemically Active Aqueous Zinc-Ion Battery Cathode. *Nano Micro Lett.* **2019**, *11*, 1–11. [[CrossRef](#)]
28. Khan, Z.; Singh, P.; Ansari, S.A.; Manippady, S.R.; Jaiswal, A.; Saxena, M. VO₂ Nanostructures for Batteries and Supercapacitors: A Review. *Small* **2021**, *17*, 2006651. [[CrossRef](#)]
29. Yang, X.; Zhang, R.; Xu, S.; Xu, D.; Ma, J.; Wang, S. Effect of carbon dimensions on the electrochemical performance of SnSe₂ anode for Na-ion batteries. *Mater. Lett.* **2020**, *284*, 128989. [[CrossRef](#)]
30. Asset, T.; Job, N.; Busby, Y.; Crisci, A.; Martin, V.; Stergiopoulos, V.; Bonnaud, C.; Serov, A.; Atanassov, P.; Chattot, R.; et al. Porous Hollow Pt/C Electrocatalysts: Carbon Support Considerations to Meet Stability Requirements. In *ECS Meeting Abstracts*; IOP Publishing: Bristol, UK, 2018. [[CrossRef](#)]
31. Ilango, P.R.; Gnanamuthu, R.; Jo, Y.N.; Lee, C.W. Design and electrochemical investigation of a novel graphene oxide-silver joint conductive agent on LiFePO₄ cathodes in rechargeable lithium-ion batteries. *J. Ind. Eng. Chem.* **2016**, *36*, 121–124. [[CrossRef](#)]
32. Liu, W.R.; Guo, Z.Z.; Young, W.S.; Shieh, D.T.; Wu, H.C.; Yang, M.H.; Wu, N.L. Effect of electrode structure on performance of Si anode in Li-ion batteries: Si particle size and conductive additive. *J. Power Sources* **2005**, *140*, 139–144. [[CrossRef](#)]
33. Wen, L.; Sun, J.; An, L.; Wang, X.; Ren, X.; Liang, G. Effect of Conductive Material Morphology on Spherical Lithium Iron Phosphate. *Nanomaterials* **2018**, *8*, 904. [[CrossRef](#)] [[PubMed](#)]
34. Yang, Z.; Kim, C.; Hirata, S.; Fujigaya, T.; Nakashima, N. Facile Enhancement in CO-Tolerance of a Polymer-Coated Pt Electrocatalyst Supported on Carbon Black: Comparison between Vulcan and Ketjenblack. *ACS Appl. Mater. Interfaces* **2015**, *7*, 15885–15891. [[CrossRef](#)] [[PubMed](#)]
35. Hench, L.L.; West, J.K. The sol-gel process. *Chem. Rev.* **1990**, *90*, 33–72. [[CrossRef](#)]
36. Iurilli, P.; Brivio, C.; Wood, V. On the use of electrochemical impedance spectroscopy to characterize and model the aging phenomena of lithium-ion batteries: A critical review. *J. Power Sources* **2021**, *505*, 229860. [[CrossRef](#)]
37. Su, F.; Tang, R.; He, Y.; Zhao, Y.; Kang, F.; Yang, Q. Graphene conductive additives for lithium ion batteries: Origin, progress and prospect. *Chin. Sci. Bull.* **2017**, *62*, 3743–3756. [[CrossRef](#)]
38. Sivonxay, E.; Aykol, M.; Persson, K.A. The lithiation process and Li diffusion in amorphous SiO₂ and Si from first-principles. *Electrochim. Acta* **2019**, *331*, 135344. [[CrossRef](#)]
39. Abate, I.I.; Jia, C.J.; Moritz, B.; Devereaux, T.P. Ab initio molecular dynamics study of SiO₂ lithiation. *Chem. Phys. Lett.* **2020**, *739*, 136933. [[CrossRef](#)]
40. Zou, G.; Wang, C.; Hou, H.; Wang, C.; Qiu, X.; Ji, X. Controllable Interlayer Spacing of Sulfur-Doped Graphitic Carbon Nanosheets for Fast Sodium-Ion Batteries. *Small* **2017**, *13*, 1700762. [[CrossRef](#)]
41. Wang, J.; Polleux, J.; Lim, J.; Dunn, B. Pseudocapacitive Contributions to Electrochemical Energy Storage in TiO₂ (Anatase) Nanoparticles. *J. Phys. Chem. C* **2007**, *111*, 14925–14931. [[CrossRef](#)]
42. Jiang, Y.; Liu, J. Definitions of Pseudocapacitive Materials: A Brief Review. *Energy Environ. Mater.* **2019**, *2*, 30–37. [[CrossRef](#)]
43. Fleischmann, S.; Mitchell, J.B.; Wang, R.; Zhan, C.; Jiang, D.-E.; Presser, V.; Augustyn, V. Pseudocapacitance: From Fundamental Understanding to High Power Energy Storage Materials. *Chem. Rev.* **2020**, *120*, 6738–6782. [[CrossRef](#)]
44. Liu, T.C.; Pell, W.G.; Conway, B.E.; Roberson, S.L. Behavior of Molybdenum Nitrides as Materials for Electrochemical Capacitors: Comparison with Ruthenium Oxide. *J. Electrochem. Soc.* **1998**, *145*, 1882–1888. [[CrossRef](#)]
45. Shen, Z.; Cao, L.; Rahn, C.D.; Wang, C.-Y. Least Squares Galvanostatic Intermittent Titration Technique (LS-GITT) for Accurate Solid Phase Diffusivity Measurement. *J. Electrochem. Soc.* **2013**, *160*, A1842–A1846. [[CrossRef](#)]
46. Liu, C.; Wu, X.; Wang, B. Performance modulation of energy storage devices: A case of Ni-Co-S electrode materials. *Chem. Eng. J.* **2020**, *392*, 123651. [[CrossRef](#)]
47. Wu, X.; Yao, S. Flexible electrode materials based on WO₃ nanotube bundles for high performance energy storage devices. *Nano Energy* **2017**, *42*, 143–150. [[CrossRef](#)]